An Automated, Objective, Multiple-Satellite-Platform Tropical Cyclone Surface Wind Analysis

JOHN A. KNAFF, MARK DEMARIA, AND DEBRA A. MOLENAR

NOAA/NESDIS Regional and Mesoscale Meteorological Branch, Fort Collins, Colorado

CHARLES R. SAMPSON

Naval Research Laboratory, Monterey, California

MATTHEW G. SEYBOLD

NOAA/NESDIS Product Implementation Branch, Camp Springs, Maryland

(Manuscript received 7 October 2010, in final form 18 May 2011)

ABSTRACT

A method to estimate objectively the surface wind fields associated with tropical cyclones using only data from multiple satellite platforms and satellite-based wind retrieval techniques is described. The analyses are computed on a polar grid using a variational data-fitting method that allows for the application of variable data weights to input data. The combination of gross quality control and the weighted variational analysis also produces wind estimates that have generally smaller errors than do the raw input data. The resulting surface winds compare well to the NOAA Hurricane Research Division H*Wind aircraft reconnaissance–based surface wind analyses, and operationally important wind radii estimated from these wind fields are shown to be generally more accurate than those based on climatological data. Most important, the analysis system produces global tropical cyclone surface wind analyses and related products every 6 h—without aircraft reconnaissance data. Also, the analysis and products are available in time for consideration by forecasters at the Joint Typhoon Warning Center, the Central Pacific Hurricane Center, and the National Hurricane Center in preparing their forecasts and advisories. This Multiplatform Tropical Cyclone Surface Wind Analysis (MTCSWA) product is slated to become an operationally supported product at the National Environmental Satellite Data and Information Service (NESDIS). The input data, analysis method, products, and verification statistics associated with the MTCSWA are discussed within.

1. Introduction

The surface wind fields of tropical cyclones (TCs) can be dramatically different, even when the maximum surface winds are very similar. Such differences can be seen in the wind field depiction by operational centers. The maximum extent of 34-, 50-, and 64-kt (1 kt = 0.514 m s^{-1}) wind radii are operationally estimated in units of nautical miles (1 n mi = 1.85 km), these will be referred to as ''gale force,'' ''damaging force,'' and ''hurricane force'' wind radii and collectively as ''operationally important radii'' throughout the remainder of the paper. The relative size of a TC's wind field also has direct implications for the potential damage a given storm may cause (Powell and Reinhold 2007; Maclay et al. 2008). Both the potential direct wind damage and the potential coastal inundation increase with the size of the wind field. In addition, the onset of gale- and hurricane-force winds occurs earlier in larger TCs, which can hamper prestorm mitigation efforts. Nature provides an example of this issue in Hurricanes Ivan (2004) and Dennis (2005). Both hurricanes had maximum wind speeds estimated near 100 kt when they approached land at nearly the same point along the U.S. Gulf Coast. Ivan, however, had a much larger wind field as indicated by operationally important wind radii estimates (Table 1) and ''H*Wind'' (Powell et al. 1998) analyses (not shown). As a consequence, the resulting damages associated with Ivan were also larger by a factor of 7 (Pielke et al. 2008).

Corresponding author address: John Knaff, NOAA/NESDIS, CIRA, Colorado State University, Campus Delivery 1375, Fort Collins, CO 80523-1375.
E-mail: john.knaff@noaa.gov

DOI: 10.1175/2011JAMC2673.1

TABLE 1. Average gale-force, damaging-force, and hurricane-force wind radii (i.e., R34, R50, and R64, respectively; km) from NHC's advisories and best tracks for Hurricanes Ivan (0600 UTC 16 Sep 2004) and Dennis (0000 UTC 9 Jul 2005) along with the Knaff et al. (2007) Atlantic climatology.

	Gale force	Damaging force	Hurricane force
Ivan	324	196	141
Dennis	237	117	65
Climatology	198	122	78

Detailed analyses like H*Wind rely to a great extent on observations taken with aircraft reconnaissance—observations that are typically limited to the western Atlantic Ocean and the region around the Hawaiian Islands. Nonetheless, the structure of the TC wind fields is routinely diagnosed at global operational forecast centers without aircraft reconnaissance. This diagnosis is often hampered by sparse in situ data and remotely sensed data from disparate sources.

In a typical operational setting there are several sources of near-surface wind data located near TCs. Examples include wind speeds from the passive microwave sensors on the Special Sensor Microwave Imager (SSM/I) (Goodberlet et al. 1989; Hollinger et al. 1987) and WindSat (Gaiser 2004), scatterometry (Graf et al. 1998; Gelsthorpe et al. 2000; Figa-Saldaña et al. 2002; EUMETSAT 2011), Advanced Microwave Sounding Unit (AMSU) nonlinear balance winds (Bessho et al. 2006), and high-resolution low-level feature-tracked winds from geostationary satellites (e.g., Holmlund et al. 2001; Velden et al. 1997, 2005). These data are all currently available in near–real time; none of these algorithms, either individually or combined, can resolve the very strong winds within 200 km or so of the TC center, however. Each individual algorithm also has its own distinct strengths and weaknesses that often make the creation of a complete surface wind analysis from any one of these individual sources untimely, complicated, unreliable, and/or difficult to interpret.

Recent work has led to techniques that can estimate analog flight-level (typically between 5000 and 10 000 ft; 1 ft $\approx$ 0.3 m) winds from infrared satellite data (Mueller et al. 2006; Kossin et al. 2007). With the addition of these new techniques, it is now possible to estimate the near-surface winds in the inner regions of TCs (i.e., wherever infrared imagery is available). These estimates can be further combined with other near-surface satellite wind estimates in the outer portions of the storm to form a multiplatform satellite-based TC surface wind analysis—one that can be automated and produced globally.

The resulting analysis system is referred to as the Multiplatform Tropical Cyclone Surface Wind Analysis (MTCSWA). The input data are described in section 2, the analysis method is presented in section 3, the operational products that are derived from the MTCSWA are summarized in section 4, and section 5 provides a verification of the wind analyses.

2. Datasets

Several satellite-based estimates of near-surface winds are used to create the MTCSWA. These estimates can be divided into two general categories: 1) wind fields created for general use and 2) those specifically created for TC problems. Winds useful for producing the MTCSWA are available at the surface (typically 10 m—marine exposure) and above the surface, typically between 925 and 600 hPa. The satellite wind estimates above the surface will hereinafter be referred to as "flight level" since these are similar to what is available from aircraft measurements. In this section, each of these data types and how they are combined to form input for the MTCSWA are discussed.

The goal of the MTCSWA is to estimate the two-dimensional field of the 1-min winds at 10-m elevation for a marine exposure. Each of the datasets used in the analysis has its own characteristics and shortcomings. Some adjustments to standardize the data, such as a surface reduction of the flight-level wind estimates, are needed. These adjustments are described below. In practice, the majority of the satellite wind estimates are located at flight level, and therefore the surface wind estimates are adjusted to a flight-level equivalent wind (a surface-to-flight-level enhancement), the objective analysis is performed, and then a flight-level-to-surface reduction is applied to the flight-level wind analysis.

a. Satellite-based surface wind estimates

The MTCSWA makes use of two satellite-based surface wind sources, and both are active radar instruments commonly called scatterometers: The SeaWinds instrument on the Quick Scatterometer (QuikSCAT) satellite[1] and the Advance Scatterometer (ASCAT; Figa-Saldaña et al. 2002; Gelsthorpe et al. 2000; EUMETSAT 2011) on the *MetOp-A* satellite. Only the oceanic wind vectors (OWV) from these platforms are used by the MTCSWA.[2] WindSat (Gaiser 2004) surface winds, although promising, are not yet utilized. QuikSCAT is a Ku-band (13.4 GHz) radar that senses ocean roughness (the

[1] QuikSCAT stopped transmitting data in November of 2009.

[2] It is also noteworthy that the *Oceansat-2* has been successfully launched and that NOAA, EUMETSAT, and the Indian Space Research Organization are now jointly working toward near-real-time distribution of the Ku-band scatterometer data.

rougher the surface is, the higher is the wind speed) and is only designed to estimate winds under approximately 30 m s^{-1}. The Ku-band frequency of QuikSCAT also has difficulties with wind direction in heavy precipitation and high winds, like those near the center of TCs (Graf et al. 1998). Hennon et al. (2006) found that OWV in the TC core region are less useful than those in the surroundings and that the QuikSCAT winds are very useful for the determination of gale-force wind radii. The ASCAT, on the other hand, is a C-band (5.225 GHz) radar that is less sensitive to precipitation than the Ku-band radar is but has lower resolution (~25 km)[3] (Gelsthorpe et al. 2000). The larger footprints of ASCAT have resulted in a bias toward lower wind speeds, particularly for high winds (Bentamy 2008; Cobb et al. 2008). For this product ASCAT surface wind speeds are increased uniformly by 5% to help reduce the low biases of those OWVs. This 5% increase of the ASCAT wind speeds also improved the correlation between ASCAT and QuikSCAT winds so that they could be treated in an identical manner (section 3). Both QuikSCAT and ASCAT attenuate at high winds, and therefore weights will be reduced when these high winds are used in the variational analysis (section 3). Gross quality control will also remove some of the winds when the attenuation occurs (section 3). Throughout the remainder of this paper "SCAT" and "ASCT" will refer to scatterometry-based winds from QuikSCAT and ASCAT, respectively.

b. Satellite-based flight-level wind estimates

1) Winds from geostationary satellites

Cloud drift feature track (CDFT) and water vapor (WV) winds from geostationary satellites are utilized at pressure levels below 600 hPa. These winds are obtained from two agencies: Fleet Numerical Meteorology and Oceanography Center (FNMOC), which provides wind fields from international agencies,[4] and the National Environmental Satellite Data and Information Service (NESDIS), which creates winds in the western/eastern Pacific Ocean and Atlantic basin. For the purposes here, winds are treated as being at one uniform pressure level (i.e., flight level) in the analysis. CDFT winds are primarily located in the region surrounding the TC because high cloud cover often prevents tracking of low-level features closer to the TC center. The number of vectors can be affected by the spectral frequency and image frequency as shown in Velden et al. (2005).

It is important to note that these winds are provided by operational centers, NESDIS and FNMOC, and reflect what is being produced and disseminated by these centers. At present, the winds provided from NESDIS are quality controlled using a recursive filter flag (Velden et al. 1997, 1998; Holmlund et al. 2001) of 50 or greater before dissemination (H. Qi 2011, personal communication). In a similar way, winds from the European Organisation for the Exploitation of Meteorological Satellites (EUMETSAT) and Japan Meteorological Agency are provided via FNMOC using the recommended (by those centers) quality indicator (QI; Holmlund et al. 2001). For instance, wind vectors created by EUMETSAT are disseminated by FNMOC if QI > 0.80, as recommended in EUMETSAT (2010). It is noteworthy that this automated quality control filters the CDFT and WV winds prior to their use in MTCSWA, whereas the other inputs are not prescreened for quality. For a more comprehensive and current review of satellite-derived winds please see the International Winds Working Group Worldwide Web pages (http://cimss.ssec.wisc.edu/iwwg/iwwg.html).

2) Advance Microwave Sounding Unit winds

Flight-level winds associated with TCs are also created from AMSU. Special processing methods have been developed for creating AMSU-based temperature profiles and geopotential height fields (Knaff et al. 2000; Demuth et al. 2004, 2006). These height fields at 700 and 850 hPa are then used to create 2D wind fields around TCs from the nonlinear balance equation (Bessho et al. 2006). To mitigate the effects of reduced resolution at the limbs of the pass, these winds are created when the center of the AMSU swath is within 700 km of the TC center location. Three satellites [*National Oceanic and Atmospheric Administration* (*NOAA*)*-15*, *NOAA-16*, and *NOAA-18*] currently provide AMSU data for this algorithm.[5] Temporal coverage is typically 1–4 times per day. An example of this type of wind field for the case of Tropical Cyclone Phet (IO032010) at 0952 UTC 2 June 2010 is shown in Fig. 1. This particular analysis was used for the 1800 UTC 2 June 2010 MTCSWA.

Notice in Fig. 1 that the winds within 100 km (i.e., 1°) of the storm center are poorly estimated because the AMSU instrument resolution is coarse (~50 km at

[3] A 12.5-km-resolution ASCAT wind product is also produced, but it is not currently being used.

[4] The Japan Meteorological Agency, the Australian Bureau of Meteorology, and the European Organization for the Exploitation of Meteorological Satellites.

[5] There are plans to use AMSU data from *NOAA-19*, *MetOp-A*, and the National Aeronautics and Space Administration *Aqua* satellite in the near future.

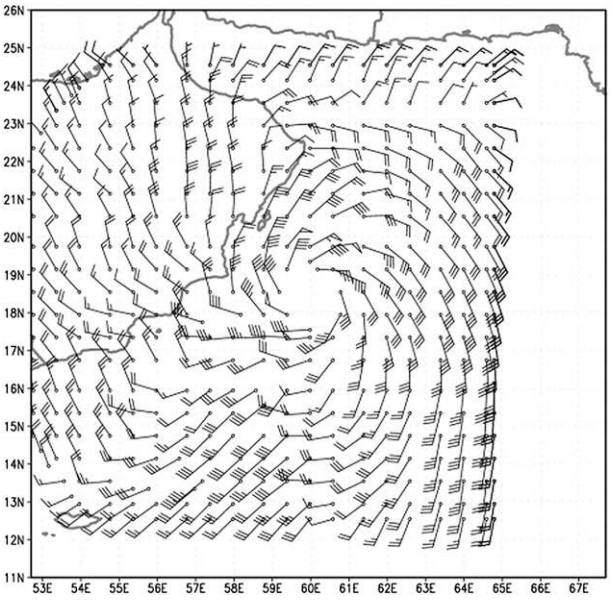

FIG. 1. Example of AMSU 700-hPa winds from Tropical Cyclone Phet at 0952 UTC 2 Jun 2010. The resolution is 0.2° lat/lon, and the winds have been thinned to show the wind barbs.

nadir). To address the issue, the MTCSWA algorithm applies lower weights to winds near TC centers. Despite the relatively low resolution, these data are useful for determining the environmental flow surrounding the TC and TC wind asymmetries.

3) INFRARED-BASED FLIGHT-LEVEL ANALOG WINDS

The winds in the inner region of the TC are estimated using a method described in Mueller et al. (2006) that has been slightly modified for this application. The technique was developed on 10 years of coincident aircraft and infrared (centered near 11 μm) (IR) imagery. Aircraft data were binned in a storm-relative manner over 12-h periods and analyzed using variational analysis in a polar framework. The IR data came from a TC satellite-image archive maintained at the Cooperative Institute for Research in the Atmosphere (Zehr and Knaff 2007). The method predicts the radius of maximum winds and wind speed at 182 km from the center (the outer radius at which aircraft data were routinely available to develop the algorithm) given the storm intensity, location, and the IR imagery. From these parameters a modified Rankine vortex is fit. Asymmetries are added to this one-dimensional wind field using the storm motion. For the MTCSWA the Mueller et al. (2006) technique was modified 1) to provide improved wind estimates in weak TCs and 2) to provide wind estimates out to 400-km radius. Details of how the Mueller et al. (2006) method was modified are provided in appendix A. These IR-based flight-level analog winds henceforth will be referred to as IRWD. In real time, the storm intensity and location are estimated using information from the most recent operational estimates and forecasts. This information comes from the National Hurricane Center, Miami, Florida; the Central Pacific Hurricane Center, Honolulu, Hawaii; and the Joint Typhoon Warning Center, Pearl Harbor, Hawaii, and is provided through the Automated Tropical Cyclone Forecast (ATCF; Sampson and Schrader 2000) databases. Extrapolation is used if no forecast information exists (i.e., typically for weaker systems that are under investigation for formation). The estimate of maximum surface wind is a source of error for the IRWDs but is necessary to provide TC structure guidance prior to the creation of the operational advisories and forecasts. The IRWD and MTCSWA analysis are intentionally generated just past the primary synoptic hours so that they are available to the centers for their operational intensity and wind radii estimates at ~1 h past the synoptic hour.

c. Data treatment

Both ASCT and SCAT winds are surface estimates (i.e., 10-m marine exposure, 1-min average), but all of the other datasets used in this study are near flight level (~700 hPa). For this reason both ASCT and SCAT data are adjusted to flight level (~700 hPa) with a conversion factor and also by rotating the winds 20° toward high pressure. Further information about flight-level-to-surface reduction and rotation factors is provided in section 3.

All of the observations used are treated in a motion-relative manner and are relocated to a common analysis time using the storm motion vector. Datasets are collected in this manner for a 12-h period prior to the analysis, except for the AMSU winds. AMSU two-dimensional winds and scatterometer winds are used for a 36-h period because they provide continuity in the outer regions of the storm. All wind types receive less weight (75% of the specified weight) if they are older than 6 h, however. Further discussion of the weights as a function of time is included in section 3. To maintain continuity from one analysis to the next, the previous analysis is used as a first guess, if available. If used, the first-guess initial wind field is given a very small weight relative to the input datasets. Last, an analysis is attempted only if IRWD input data exist.

d. Validation/comparison datasets

The H*Wind analysis system (Powell et al. 1998, 2010) is an integrated TC observing system. H*Wind uses

wind measurements from a variety of observation platforms to create an objective analysis of the distribution of wind vectors in TCs. Platforms used in these analyses include aircraft reconnaissance flight-level winds, stepped-frequency microwave radiometer (SFMR) surface wind estimates, surface stations, ships, buoys, QuikSCAT, and feature track winds. H*Wind analyses provide a unique dataset, one that is heavily weighted toward aircraft-based observations, for validating the MTCSWA.

In addition to the H*Wind analyses, the ATCF best tracks, which include postseason reanalyzed intensity, positions, and operationally important wind radii, are used for the validation of the MTCSWA. ATCF best-track wind radii have been reanalyzed in postseason since 2004 at the end of each hurricane season (NHC 2011).

3. Analysis method

The multiplatform, storm-relative, flight-level dataset described in section 2 is used as input to an objective analysis system. The MTCSWA objective analysis (a type of variational analysis) is based upon the model-fitting approach with smoothness constraints described by Thacker (1988). In this approach, the difference between the data and the model counterpart of the data is minimized, where the model is simply the wind components on any evenly spaced grid. The model counterpart of the observations is a bilinear interpolation of the wind components to the location of the observation. The smoothness constraints help to fill in the data-void areas of the analysis domain.

As an example, suppose there are K observations of wind components u and v, denoted by u_k and v_k, and M observations of wind speed, denoted by s_m, located at arbitrary locations with a domain $x \in [0, L_x]$, $y \in [0, L_y]$, where L_x and L_y define the size of the upper boundary of the x and y domain, respectively. For the objective analysis, the values of u, v, and s on an evenly spaced x, y grid with grid spacing of Δx, Δy (denoted by U_{ij} and V_{ij}) are determined by minimizing the cost function C defined by

$$C = \frac{1}{2}\sum_{k=1}^{K} w_k[(u_k - U_k)^2 + (v_k - V_k)^2] + \sum_{m=1}^{M} w_m(s_m - S_m)^2 + \sum_{i=1}^{I}\sum_{j=1}^{J}\{\alpha[(\delta_{xx}U_{ij})^2 + (\delta_{xx}V_{ij})^2] + \beta[(\delta_{yy}U_{ij})^2 + (\delta_{yy}V_{ij})^2]\}, \quad (1)$$

where δ_{xx} and δ_{yy} are the discretized second-derivative operators defined by

$$\delta_{xx}U_{ij} = (U_{i+1,j} + U_{i-1,j} - 2U_{ij})/\Delta x^2 \quad \text{and}$$

$$\delta_{yy}V_{ij} = (V_{i+1,j} + V_{i-1,j} - 2V_{ij})/\Delta y^2,$$

respectively.

In (1), U_k and V_k are the component wind values bilinearly interpolated from the analysis grid to the observation point k, w_k are data weights, the terms α and β are smoothness constraints, and I and J are the number of analysis points in the x and y directions. In a similar way, S_m are the wind speed values interpolated to the observation point m and w_m are the data weights for the wind speed. The first two terms on the right side of (1) measure the misfit between the analysis and the observations, and the third term is a constraint that acts as a low-pass filter. As shown by DeMaria and Jones (1993) for the one-dimensional case, the filter response function $F(k)$ for the constraint term in (1) can be written as

$$F_k = 1/\{1 + 8\alpha[1 - \cos(k\Delta x)]^2\}, \quad (2)$$

where $F(k)$ is the amplitude reduction factor of a pure cosine wave with wavenumber k. Because α is in the denominator in (2), increasing that parameter increases the amount of smoothing. For example, for the $2\Delta x$ wave on the analysis grid ($k = 2\pi/2\Delta x$), the amplitude will be reduced by a factor of $(1 + 32\alpha)^{-1}$. Thus, α and β can be chosen to be consistent with the data coverage relative to the analysis grid spacing. In the analysis code, the fields U_{ij}, V_{ij}, and S_{ij} that minimized C are found using a simple steepest descent algorithm, which requires calculation of the gradient of C with respect to U_{ij} and V_{ij}. Given the simple form of (1), the gradient is calculated using an analytic formula.

The objective analysis for the MTCSWA is formulated in polar coordinates with 201 radial points (Δr = 4.5 km) from r = 2 km to r = 902 km (i.e., the upper boundary of the X domain L_x is 902 km) and 36 azimuthal points ($\Delta\theta = 10°$) so that the upper boundary of the Y domain L_y is 360°, and the wind components are input as radial and tangential values. An advantage of the polar system is that different smoothness constraints can be applied in the radial and azimuthal directions.

Different weights (i.e., w_k and w_m) are also applied to the datasets when applying the cost function in (1). Weights of the individual data types are estimated and given simple functional forms based on the average errors with respect to the H*Wind (Powell et al. 1998) analyses. To keep the analysis weights relatively simple, H*Wind datasets collected during 2005, 2006, and 2007 were stratified by intensity and then compared with the input datasets to estimate the errors associated with the

input as a function of radius and intensity. AMSU, WV, and CDFT inputs have constant weights. IRWD and SCAT weights are functions of both radius r and maximum winds (vmax). To facilitate the estimation of weights we define the functional forms

$$\begin{aligned} \text{vf} &= 1 + (\text{vmax} - 50)/65, \\ \text{wt}_{\text{ir}} &= 0.35\text{vf}, \\ \text{wt}_{\text{scat}} &= 0.45\text{vf}, \quad \text{and} \\ \text{dist}_{\text{scat}} &= 50\text{vf}, \end{aligned} \tag{3}$$

where $\text{dist}_{\text{scat}}$ has units of kilometers. The weights for AMSU, WV, and CDFT winds are set to the constants 0.13, 0.3, and 0.3, respectively. The weights for the IRWD are defined by

$$W_{\text{irwd}} = \text{wt}_{\text{ir}} - 0.000\,125r \times (\text{vf})^2, \tag{4}$$

which decrease with increasing radius and have smaller values for storms with maximum intensities of less than 50 kt. The weights for SCAT/ASCT winds are defined by

$$\begin{aligned} W_{\text{scat}} = \min[0.60, \text{wt}_{\text{scat}} + \text{vf}(r - \text{dist}_{\text{scat}}) \\ \times 0.0004], \quad r \geq \text{dist}_{\text{scat}}. \end{aligned} \tag{5}$$

For the SCAT/ASCT winds occurring within $\text{dist}_{\text{scat}}$ of the TC center, the wind speed weights [i.e., w_m in (1)] are equal to the wt_{scat} and the weights for the wind speed components [i.e., w_k in (1)] are set to 0. Examples of the wind component weights and wind speed weights for each product are shown as a function of radius for three different intensities in Fig. 2.

Notice that scatterometry-based winds are generally weighted most in the analysis and increase as a function of radius. IRWD inputs also have fairly large weighting in the analysis and decrease as a function of radius. SCAT/ASCT and IRWD weights also decrease and increase, respectively, near the storm center and with higher intensities. CDFT/WV winds are weighted relatively heavily but are very often unavailable near the TC center. The AMSU-based winds receive only moderate weights but are routinely available for the entire domain. The larger relative weights used for the SCAT/ASCT OWVs is noteworthy, implying these are the winds with the lowest errors. Results also suggest that OWVs in the TC core region are less reliable for stronger TCs, so that the findings in Hennon et al. (2006) were very likely based on a sample of stronger TCs.

The variational analysis is actually run three times, which allows for some additional quality control. The first analysis uses fixed smoothing constraints α and β in (1). Using this first relatively smooth analysis, a gross quality control is applied to remove obviously errant data from subsequent analyses. For the two remaining analyses, α and β in (1) are chosen so that the half-power wavelengths of the filter were 22.5 km in radial direction and 100° in azimuth within 300 km of the center, becoming equally weighted when 500 km or greater from the center, where half-power filter weights are ~350 km in both directions. Again a gross quality control is applied

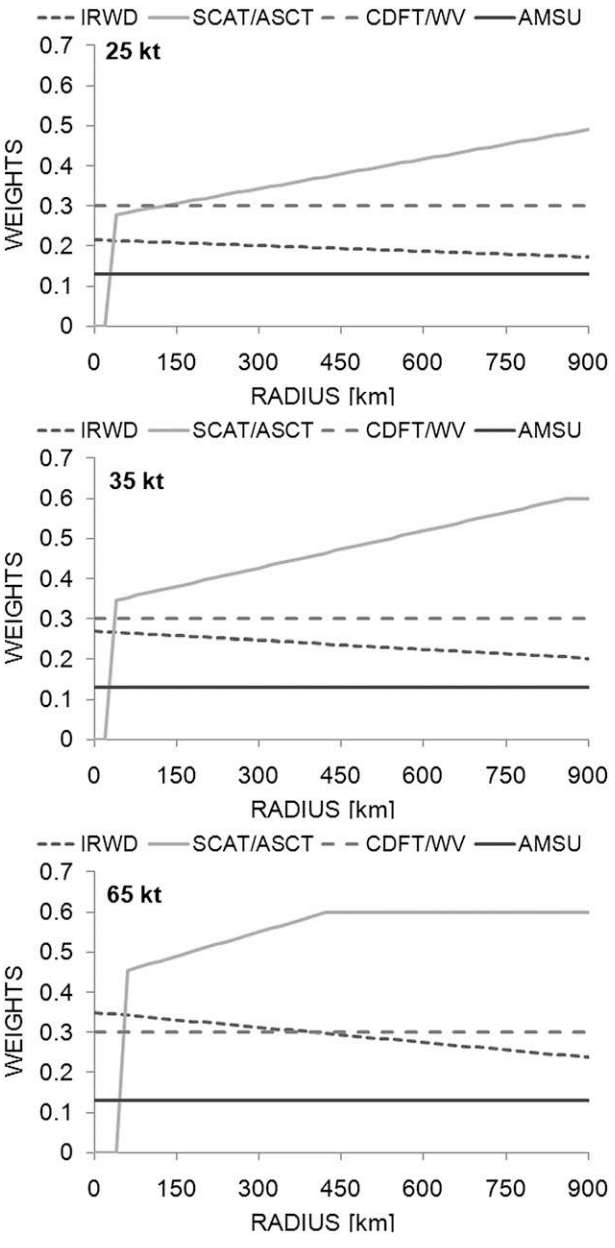

FIG. 2. Examples of data weights as a function of data type, radius, and intensity. Note that all weights for storms with intensities greater than 65 kt have weights that are the same as those in the bottom panel.

TABLE 2. Gross quality control applied between the second and final analyses; V_{max} here is given in units of meters per second.

Gross quality-control pass	Function
First—prior to the second analysis	Max(3.6, $0.103V_{max}$)
Second—prior to the final analysis	Max(1.8, $0.051V_{max}$)

between the second and final analysis. For each quality-control step, the threshold for the quality control is a function of the maximum observed wind speed in the data as shown in Table 2. If the magnitude of the difference between the analysis wind vector interpolated to the observation point and the observation wind vector exceeds the threshold, the data weights are simply set to 0 for that data point.

Once the various satellite wind data are analyzed to a common level (at ~700 hPa), a simple marine exposure surface wind reduction is applied (i.e., to estimate the 10-m, 1-min wind vectors). Based on the findings of Franklin et al. (2003) and assuming a convectively active TC, the flight-level-to-surface wind speed reduction factors of 0.9 within 100 km of the TC center and 0.75 beyond 700 km from the TC center are used. Between 100 and 700 km, the reduction factor decreases linearly to a value of 0.75 at 700 km. The resulting winds are also turned toward low pressure by 20°, which is an approximation to the turning angles found in the dropwindsonde data used in the Franklin et al. (2003) study (J. Franklin 2009, personal communication). A land mask is then used to determine whether the observation is over land. If the wind observation is over land, an additional 25% reduction (i.e., the marine exposure wind speed is multiplied by 0.80) is applied and the wind speed and the vectors are turned an additional 20° following Boose et al. (2001), for a total turning of 40°. The flight-level-to-surface reduction factors for locations over water and over land are shown in Fig. 3 as a function of radius. No special treatment is applied to the winds as they approach or leave the ocean–land interface (i.e., they are either treated as being over land or over water).

Last, minimum sea level pressure (MSLP) estimates are created by integrating the resulting azimuthally averaged wind at flight level (considered to be gradient level) from 600 km inward. The inward integration starts with the azimuthally averaged sea level pressure at 600 km that is provided by the National Centers for Environmental Prediction Global Forecast System (GFS) model analysis.

4. Operational product description

The MTCSWA product is disseminated through the product Internet site (http://www.ssd.noaa.gov/PS/TROP/mtcswa.html). The products range from graphical

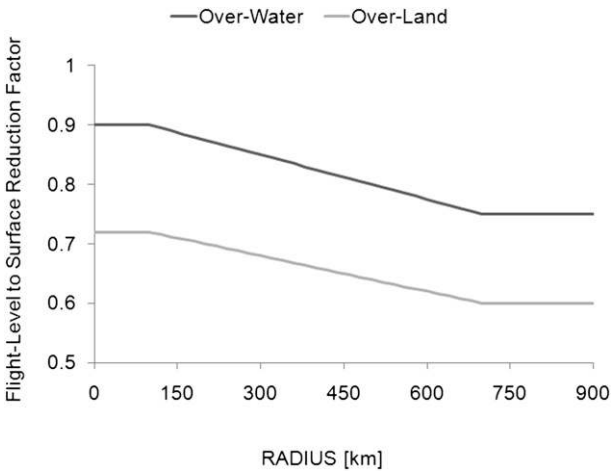

FIG. 3. The flight-level-to-surface reduction factors used in MTCSWA for overwater and overland conditions.

information to text data and include all of the information needed to reprocess the input data. A short-term (~1 month) archive of these products is available through a file-transfer protocol (ftp) link on the Worldwide Web page. An archive agreement has also been established with the National Climatic Data Center (NCDC) to archive all graphical and text products.

a. *Graphical products*

There are nine graphical products. These include eight products displayed on the Web page (http://www.ssd.noaa.gov/PS/TROP/mtcswa.html): the surface wind analysis (storm scale), the surface wind analysis (inner-core scale), AMSU data used in the analysis, CDFT/WV data used in the analysis, IRWD data used in the analysis, SCAT/ASCT data used in the analysis, a time series of maximum winds and MSLP, and an infrared image of the TC at analysis time. The final graphical product also provides the kinetic energy (KE) within 200 km of the cyclone center at flight level, plotted against the intensity. The scale for KE is provided in Maclay et al. (2008) and has been related to damage potential. Examples of the graphical products for Hurricane Celia (EP0410) at 0000 UTC 21 June 2010 are shown in Figs. 4 and 5.

b. *Text products*

A number of ancillary data files are also generated that contain input, output, and diagnostic information. A complete list of files included in the archive is listed in appendix B. One text file created, the ATCF formatted fix, is of particular interest to operational users. This file appears in the archive but is also posted for a short duration (~1 day) in a location from which operational centers can then retrieve it by ftp in real time. This nearly instant availability will allow the MTCSWA fix information to be

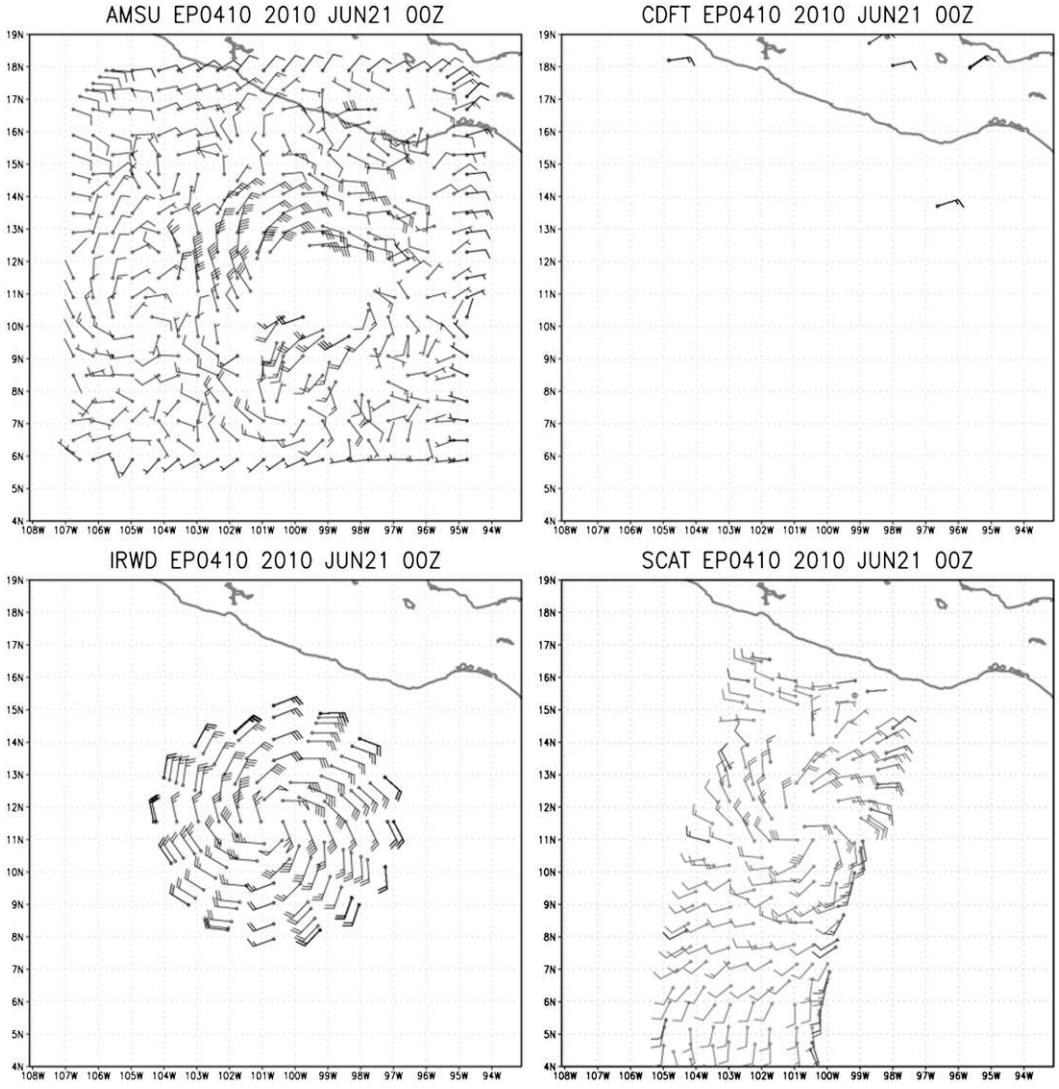

FIG. 4. Examples of graphical products generated for Hurricane Celia (EP0410). Shown are the basic input datasets: AMSU, CDFT, IRWD, and ASCT.

considered in operational TC advisories and forecasts, which are often prepared in the first hour after 0000, 0600, 1200, and 1800 UTC (Rappaport et al. 2009).

5. Product verification

Because TC surface wind field estimates are considered to be most accurate when aircraft reconnaissance is available, the MTCSWA is verified using two different datasets. The first dataset is the H*Wind analyses (Powell et al. 1998, 2010) obtained from the NOAA Hurricane Research Division. The H*Wind analyses of the two-dimensional wind field make use of surface winds from buoys, station observations, ships, and satellite cloud-drift winds in addition to aircraft reconnaissance data at flight level and at the surface by means of SFMR. The second verification dataset is the operationally important wind radii and MSLP from the best-track analyses from NHC. The operationally important wind radii and MSLP estimates from climatological data (hereinafter referred to as ''climatology'') are also included in this second verification. The wind radii climatology is from Knaff et al. (2007) and the MSLP climatology is computed from maximum wind speed using the Dvorak (1975) Atlantic wind–pressure relationship provided in Knaff and Zehr (2007). Both verifications were conducted during 2008–09 when the MTCSWA algorithm was static and SFMR surface wind estimates were operational.

It is noteworthy that operational TC intensities and wind radii are reported in units of knots and that operationally

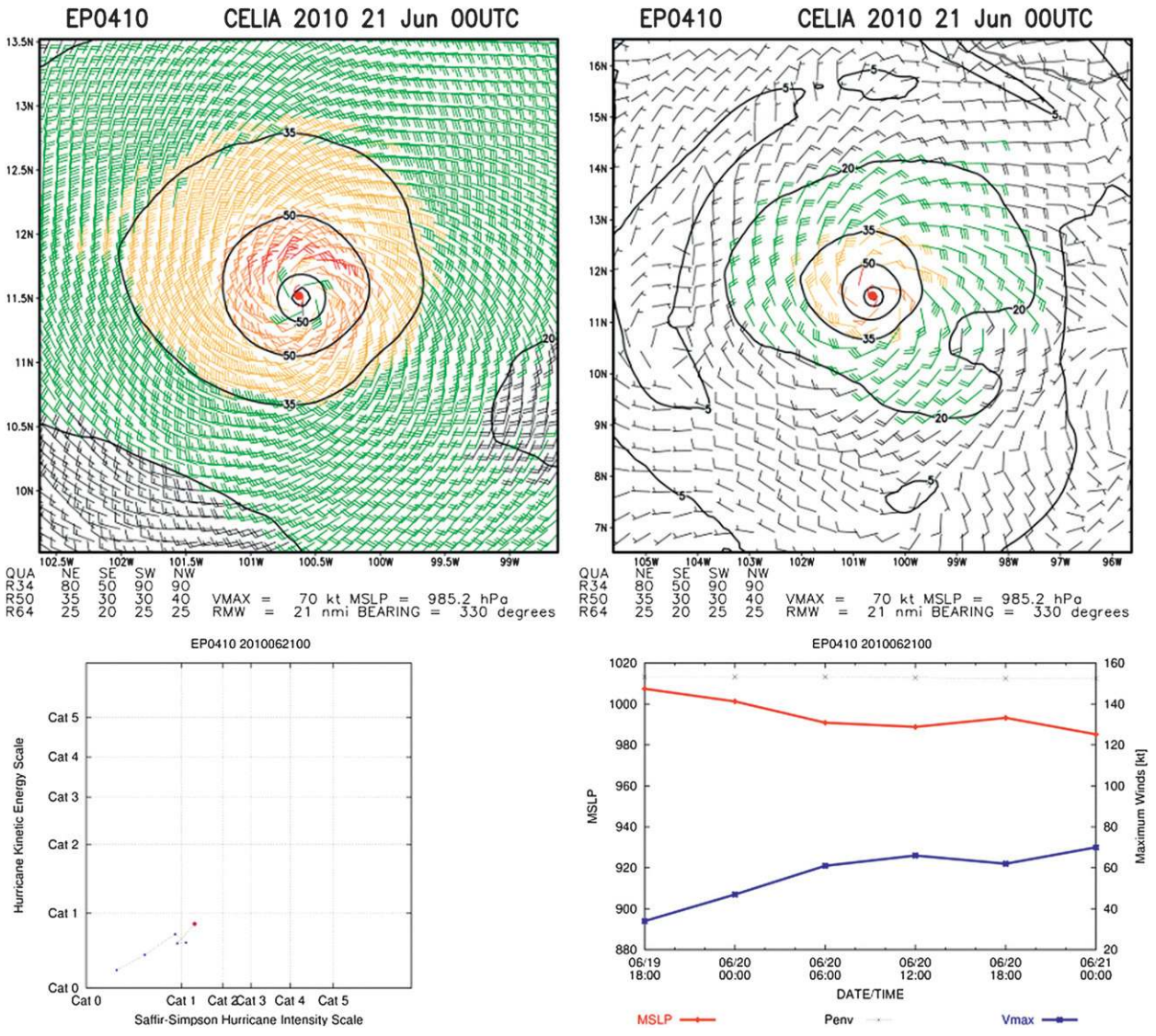

FIG. 5. Examples of MTCSWA products generated for Hurricane Celia (EP0410). Note that these products have non-SI units that are used in operations. (top) The wind analysis is created at two different scales. Also shown are (bottom left) the time series of the integrated kinetic energy (0–200 km) vs current intensity and (bottom right) the time series of the analyzed maximum wind speed (kt) and estimated MSLP (hPa).

important wind radii are reported in units of nautical miles. As a result, the MTCSWA outputs are given in those units and thus the examples (Figs. 4 and 5) shown are in those units. When comparing the analysis and wind radii results, we conform to the international system of units (SI).

*a. H*Wind comparisons*

Comparisons between MTCSWA and H*Wind analyses were conducted in a storm-relative coordinate system. The closest H*Wind analysis with respect to time was used for the comparisons. The polar-grid results of the MTCSWA were compared with H*Wind analyses interpolated to the same polar coordinate system. Spatial mean absolute errors (MAE) and biases were then calculated. In the 2008–09 period there were 250 coincident H*Wind and MTCSWA analyses in the Atlantic and eastern Pacific Oceans, which not only provided a large representative sample of cases for our analysis but also allowed further stratification by intensity.

Figure 6 shows the MAEs and biases associated with the analysis of all 250 coincident cases. The MAEs are the largest within approximately 60 km of the center of the cyclone, where errors exceeded 5 m s^{-1}. Elsewhere,

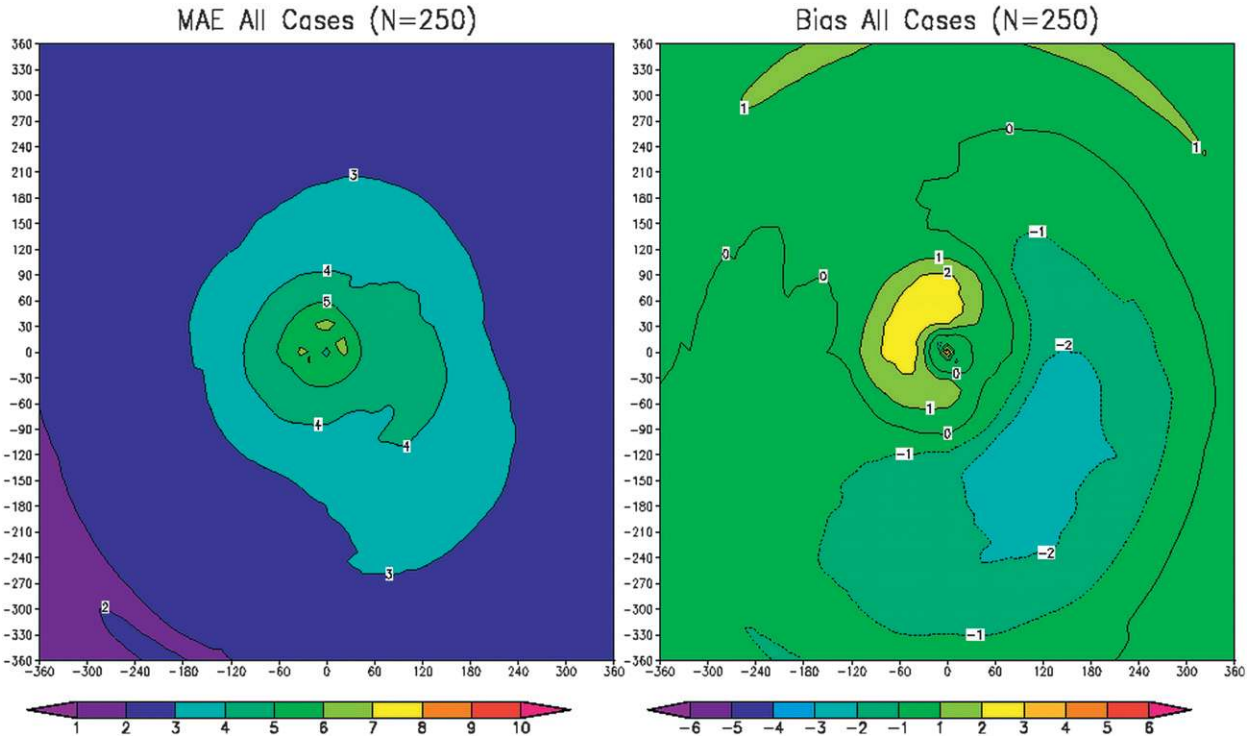

FIG. 6. The (left) MAEs and (right) biases associated with the MTCSWA for all cases with coincident (±3 h) H*Wind analyses. H*Wind is assumed to be ground truth, and the centers of the two analyses are collocated for analysis purposes. Units are meters per second.

MAEs are smaller than 5 m s^{-1} and appear to be roughly symmetric about the storm center. The biases show a tendency to overestimate slightly in the northwest quadrant of the storm within 100 km and to underestimate slightly the winds on the southeast quadrant between approximately 120 and 250 km from the storm.

We next examine the MAEs and biases as a function of TC intensity. Figure 7 shows MAEs and biases for nonhurricane cases (<33 m s^{-1}) (top panels), and hurricane (≥33 m s^{-1}) cases (bottom panels). The maximum wind in each H*Wind analysis is used to stratify the cases.

The nonhurricane cases (Fig. 7, top panels) show that the majority of the domain has MAE of less than 5 m s^{-1}. The largest MAEs occur in the regions where the radius of maximum wind (RMW) would most likely also occur. In shifting focus to the biases associated with the nonhurricane cases, it is seen that there appears to be a wavenumber-1 bias pattern with positive biases in the northwest quadrant between 30 and 120 km and negative biases occurring on the southeast side of the storm between 120 and 250 km. There is also an indication that the winds near the center of these weaker storms may be slightly underestimated.

The hurricane cases (Fig. 7, bottom panels) show that the MAEs exceed 5 m s^{-1} within approximately 60 km of the center. Upon closer examination, it is seen that much of this error is associated with three issues. The first is that the RMW estimated from the IRWD techniques is unable to resolve the very small eyes that occasionally occur. In fact, the smallest RMW that this technique is able to estimate is about 9 n mi (16 km), given the IR image resolution. The second issue is that the IRWD technique fits a Rankine vortex to the wind field from the RMW to 182 km from the center. This assumption does not allow for the rapid decrease of winds outside the radius of maximum winds that is sometimes observed in very intense TCs. Third, the IRWD technique cannot account for multiple RMW or eyewalls. When multiple eyewalls occur the technique tends to estimate a RMW between the two possibilities. Biases for the hurricane cases show a wavenumber-1 pattern that is similar to that of the nonhurricane cases, but with a slightly larger magnitude.

The consistent wavenumber-1 patterns in the biases away from the inner core suggest that one of the input datasets is the likely cause. Upon further examination, the AMSU winds are found to be responsible for the pattern in the bias. Although the AMSU is the source of the pattern in the biases, the cause of the pole-to-equator bias difference in the AMSU winds has yet to be resolved. Note also that, because the product is available

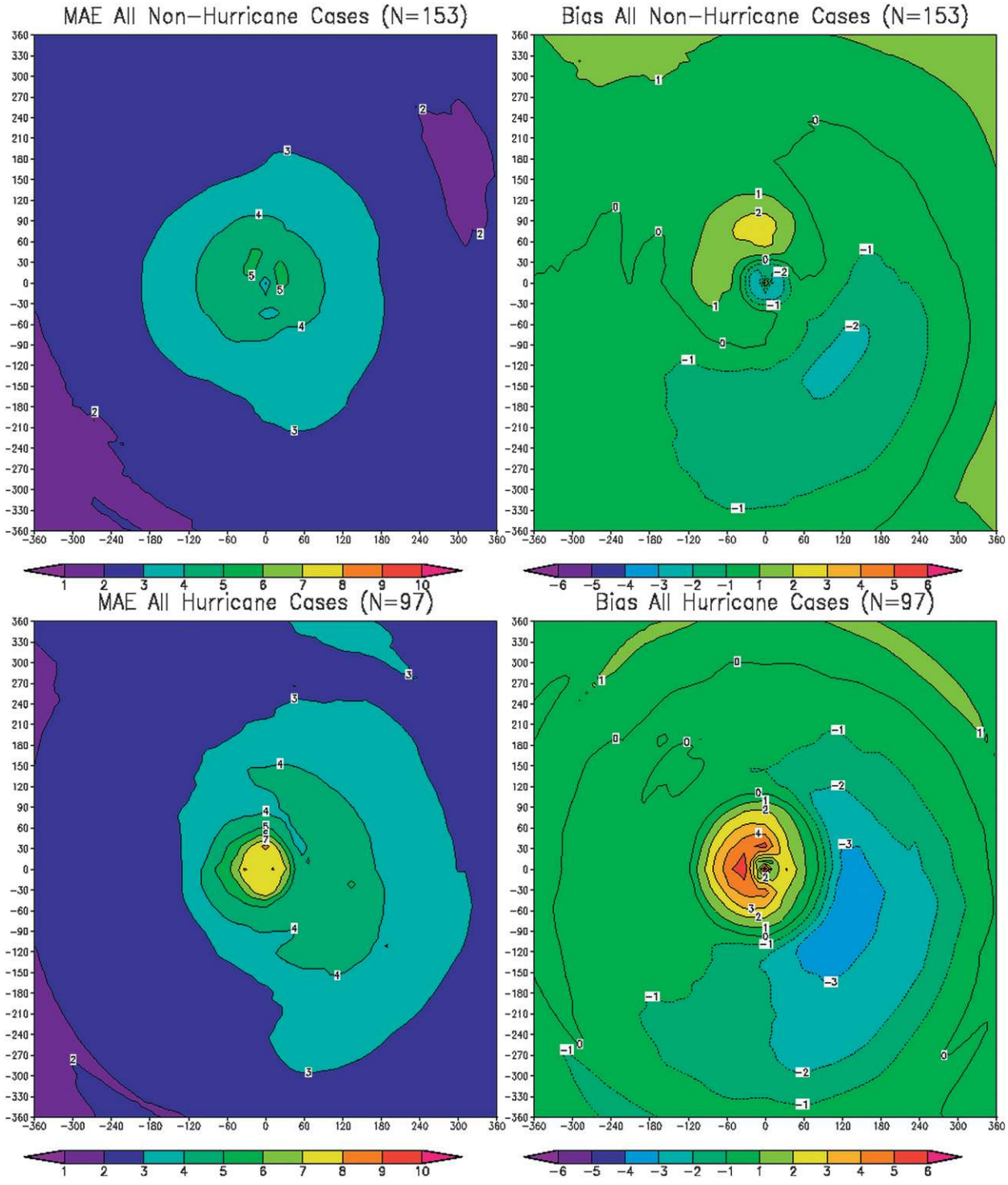

FIG. 7. As in Fig. 6, but for (top) nonhurricane cases and (bottom) hurricane cases.

in time for consideration for the forecasts, the estimated intensity used for the IRWD is an additional source of error that occurs most often when rapid changes of intensity are poorly anticipated from one forecast time to the next. It is possible that these errors could be minimized if operational estimates of intensity, which blend the subjective and objective intensity estimates, were more frequent or were available slightly earlier.

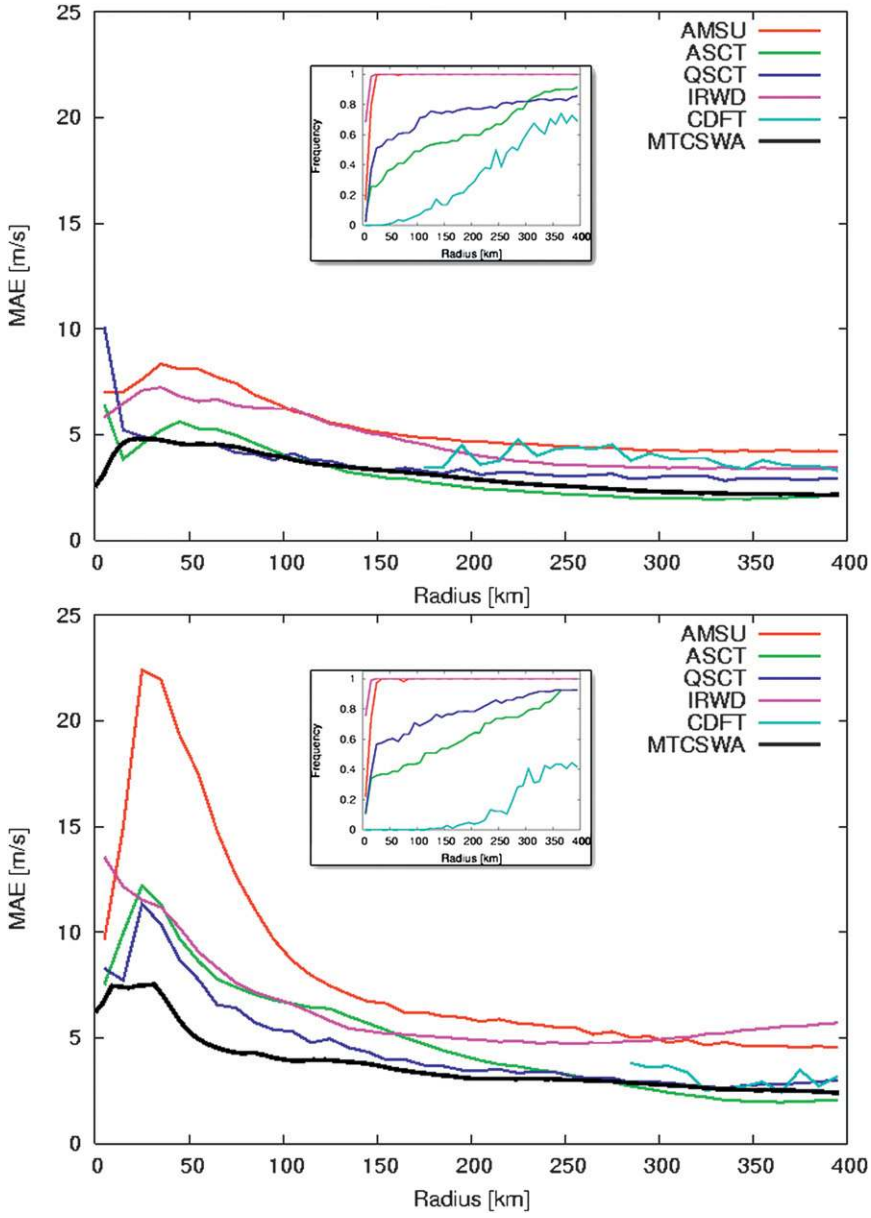

FIG. 8. Azimuthally averaged MAE associated with the input datasets used in the MTCSWA and the final MTCSWA analyses: (top) nonhurricane cases (<33 m s^{-1}) and (bottom) hurricane cases (≥ 33 m s^{-1}). The frequency of the data types as a function of radius is provided in the respective inserts. H*Wind cases are used as ground truth, and the same 2008–09 sample is used.

To complete this analysis, it is informative to compare the above results with the MAEs associated with the raw input data used in the MTCSWA. Figure 8 shows the azimuthal mean MAEs associated with the five of the inputs [IRWD, AMSU, ASCT, SCAT (i.e., QSCT in Fig. 8), and CDFT] and for the MTCSWA for nonhurricane cases (top panel) and hurricane cases (bottom panel). The MAE values for input data are not shown in Fig. 8 if the number of points is less than 30. This comparison, which uses the same cases used in Figs. 6 and 7, clearly shows that the MTCSWA product produces MAEs that are generally smaller than any of the individual inputs, and thus not only does it combine the input data information but it adds value by decreasing the potential analysis errors.

b. *Wind radii and MSLP comparisons*

Using the 2008–09 data sample, we compare the MTCSWA-based operationally important wind radii

and MSLP estimates with the estimates in the best-track files and those estimated from climatology. The best-track files contain the best estimates of intensity, MSLP, and operationally important wind radii associated with a given TC with a 6-hourly frequency. Because there are relatively few tools to estimate wind radii, errors associated with the best-track estimates may be as high as 25%–40% (Knaff and Harper 2010). These comparisons were nonetheless calculated for all Atlantic[6] cases within ±2 h of aircraft observed/estimated MSLP in 2008 and 2009. The verification considers wind radii in the individual quadrants (northeast, southeast, southwest, and northwest) as well as the averages all quadrants. It is important to note that, even with aircraft reconnaissance, the extent of gale-force winds is sometimes larger than the typical radial flight leg, which is approximately 185 km. Also because of the stepped nature of wind radii measurements, the all-quadrants wind radii evaluation compares the average of the nonzero wind radii and thus is a general measure of TC size. Many statistics were calculated [MAE, bias, RMSE, percent variance explained (R^2), false-alarm rate F, and probability of detection (POD)]. For simplicity, however, this discussion will concentrate on the MAE, bias, and R^2 statistics for the sample for which aircraft were available to emphasis MTCSWA performance versus climatological estimates of both operationally important wind radii and MSLP (as a function of intensity). Note that the MAE verification results include wind radii estimates of zero (i.e., no wind radii in the quadrant).

Figure 9 shows the MAEs and biases of the radii of gale-force, damaging-force, and hurricane-force wind radii for which aircraft observations were available. Observational units are converted to SI units, where 1 n mi = 1.85 km. The MTCSWA-based wind radii estimates generally perform better than climatology, especially for the hurricane-force and damaging-force wind radii. Negative biases in the east quadrants shown in the H*Wind comparisons carry over to the underestimates of the wind radii in the northeast and southeast quadrants in Fig. 9. It is interesting to note, however, that climatology has similar biases. This result highlights the sensitivity of wind radii estimates to the analyzed wind speeds in that small radial changes in wind speed can result in very large differences in wind radii estimates. The hurricane-force wind radii also show a tendency to have a slight positive bias (values are too high) as would be expected as a result of errors associated with the radius of maximum wind shown in the previous section and the known limitations of the IRWD input data, but MTCSWA biases still show some improvements over climatology.

The MTCSWA-based operationally important wind radii generally explained larger amounts of variance than their corresponding climatological estimates, shown in Fig. 10. This result even holds true for the hurricane-force wind radii. This finding indicates that the MTCSWA-based wind radii that are provided capture important additional aspects about the asymmetries of the wind fields around TCs much better than does the climatology. The larger variance explained by the nonzero averaged wind radii (labeled ALL in the plots) also indicates that MTCSWA captures more of the general vortex size variations.

The F and POD statistics for the MTCSWA and climatological estimates of operationally important wind radii (not shown) provided some additional information about the characteristics of the MTCSWA. The Pierce skill score (PSS), which can be calculated as POD minus F and measures the ability to discriminate yes cases from no cases, showed that in general both the MTCSWA and climatology had skill for all quadrants and all wind thresholds. The MTCSWA outperformed climatology by the PSS measure by 20%, 25%, 6%, and 7% for northeast, southeast, southwest, and northwest damaging-force wind quadrants and two of the four gale-force quadrants (0%, −54%, 63%, and 89%, respectively). For hurricane-force wind radii, climatology had better PSS for all but one of the quadrants (0%, −67%, −23%, and −18%, respectively). Similarly, MTCSWA had larger PSSs than climatology for detecting of gale-force (87%), and damaging-force (7%) winds in any quadrant, but climatology had a slightly better PSS for detecting of hurricane-force wind radii (−20%).

The final parameter examined in this analysis was the MSLP. To do this we used the Dvorak (1975) Atlantic wind–pressure relationship as climatology, which is the accepted climatological relationship for the Atlantic basin. We then compared those values with estimates made by integrating the azimuthal mean wind field produced by the MTCSWA to estimated ΔP and MSLP. Table 3 shows that the MTCSWA provides slightly improved estimates of MSLP with very small biases. Furthermore, because the MSLP is an integrated measure of the wind, this result also indicates indirectly that the MTCSWA is producing a dynamically consistent wind field.

6. Summary and conclusions

A technique (MTCSWA) that creates estimates of surface wind fields around tropical cyclones using only satellite-based information has been described. Input

[6] Because we do not want to mix basin climatologies, this analysis was conducted with only the Atlantic cases available in these years.

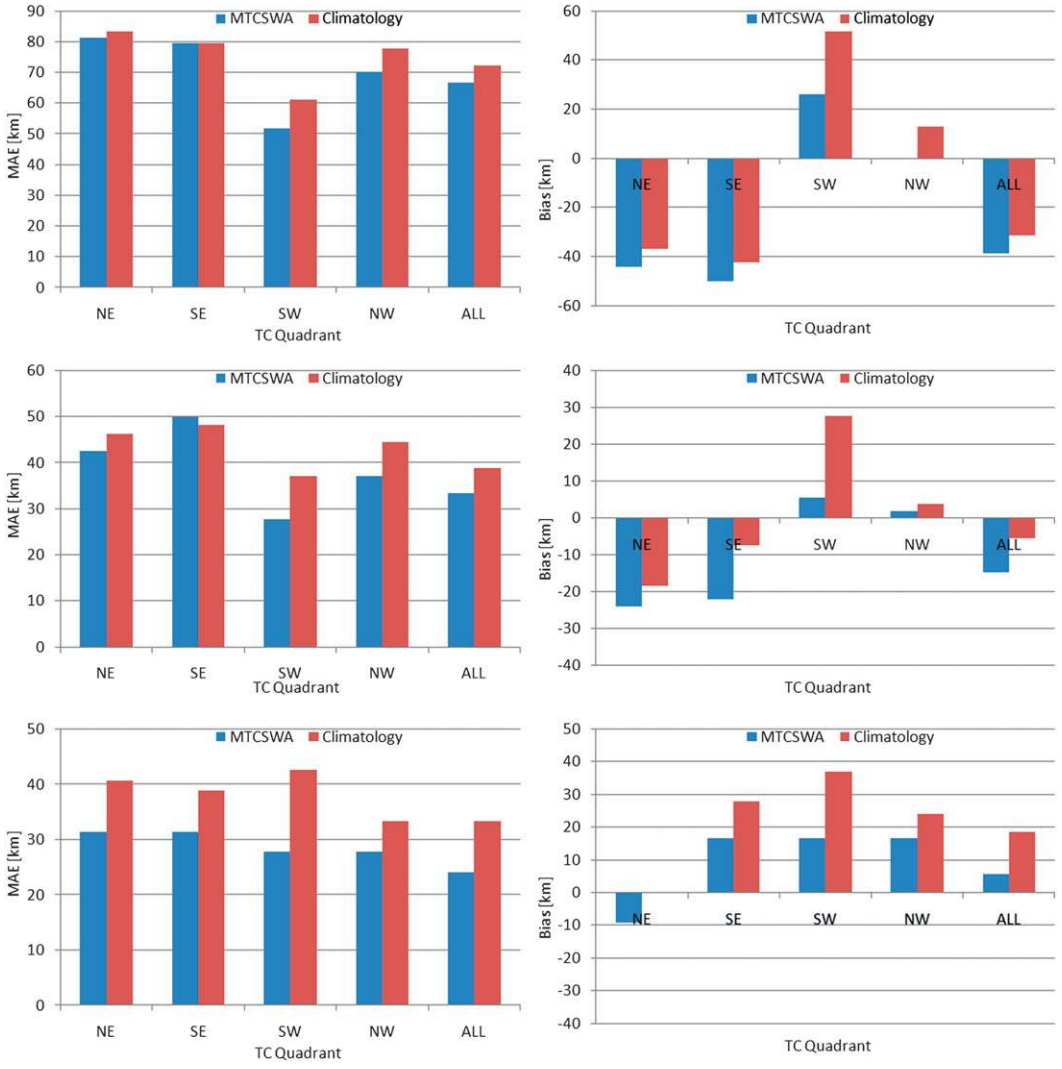

FIG. 9. (left) MAE and (right) bias associated with the wind radii estimates of the MTCSWA product and that of climatology for the (top) gale-force, (middle) damaging-force, and (bottom) hurricane-force wind radii. The number of cases analyzed is 129, 79, and 59, respectively.

datasets include several routinely available near-surface wind data types and an IR-based flight-level wind analog. The MTCSWA analysis is conducted on a polar grid and allows for differential smoothing factors to be applied in the radial and azimuthal directions, variable data weights, and inclusion of speed-only wind information. Gross quality control of the input data is also performed using intensity-based thresholds (Table 2).

The MTCSWA analyses are shown to have MAEs that are less than 5 m s^{-1} over most of a 400 km $\times$ 400 km domain centered on the storms, using H*Wind analyses as ground truth. The use of variable weights on input data and gross quality control results in an additional reduction in analysis errors, producing generally lower errors than the input data alone. MTCSWA estimates of operationally important wind radii generally outperform those of climatology and show reasonable ability to capture analysis-to-analysis changes in these wind radii and size changes. Estimates of MSLP, an integral measure of the wind field, also showed lower errors than did climatological estimates based on maximum winds.

Because this analysis system does not rely on aircraft-based reconnaissance data, it produces wind field estimates for the entire global suite of TCs. The analysis and products (i.e., less than an hour after synoptic time) provide timely information that can be utilized in the operational forecasts, which are completed by 3 h after synoptic time at U.S. TC warning centers. Furthermore, because most TC basins lack routine aircraft reconnaissance, these analyses and products could be used by

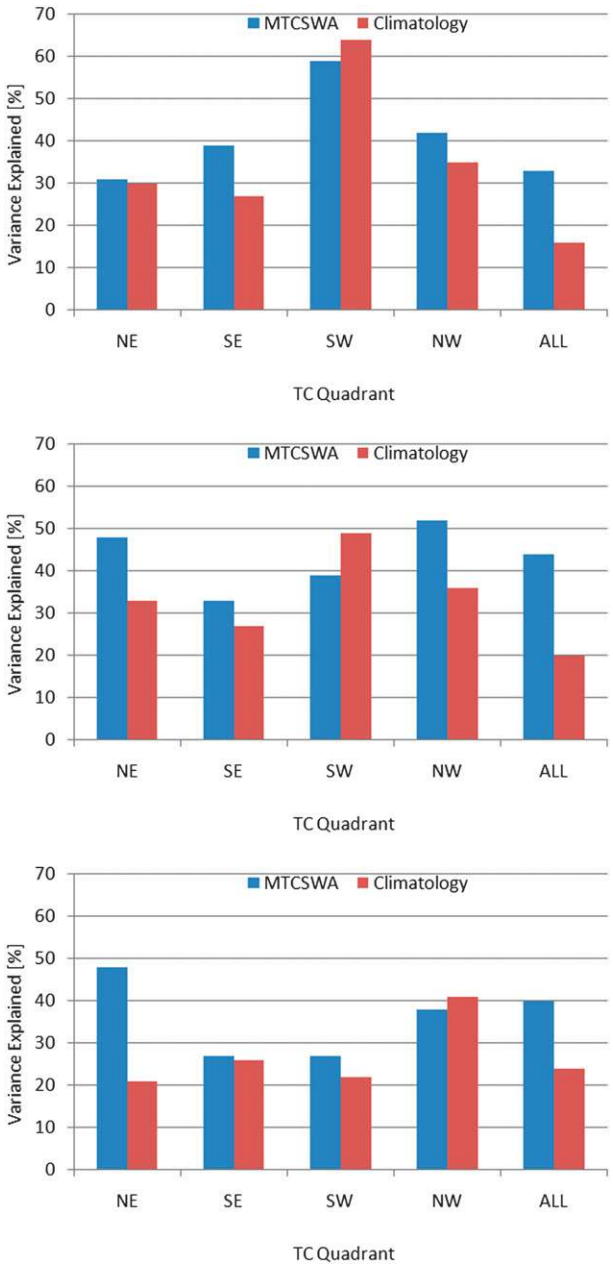

FIG. 10. Percent variance explained by wind radii estimates from the MTCSWA product and from climatology (Knaff et al. 2007) for (top) gale-force, (middle) damaging-force, and (bottom) hurricane-force wind radii.

TC warning centers throughout the world to assess TC wind structure.

This analysis system and related products (see Figs. 4 and 5 and Table B1) will soon be an operational product run and supported at NESDIS. Products will be posted online (http://www.ssd.noaa.gov/PS/TROP/mtcswa.html). For the forecasters using ATCF databases, the analysis fixes that contain the wind radii estimates are provided in real time through ftp sites so that the various operational centers can retrieve them in a timely manner. The real-time products will be archived at the National Climatic Data Center.

TABLE 3. The verification statistics (hPa) comparing the MSLP estimated by the MTCSWA product with those estimated from the Dvorak (1975) climatology.

	MTCSWA	Climatology (Dvorak 1975)
Bias	0.5	2.4
MAE	6.8	7.0
RMSE	9.5	9.2
R^2 (%)	84	82

Acknowledgments. This project is supported by NOAA Grant NA17RJ1228 with funding from the GOES Improved Measurements and Products Assurance Plan (GIMPAP) and GOES Product Services Development and Improvement (PSDI) program. The fourth author thanks NOAA's Hurricane Forecast Improvement Program (HFIP), which funded his efforts. The authors also thank the NOAA Hurricane Research Division of AOML (and Dr. Mark Powell and Shirley Murillo) for maintaining and sharing H*Wind analyses of past TCs and thank Hongming Qi (NESDIS) and Paul McCrone (U.S. Navy) for providing details concerning the filtering associated with cloud drift and water vapor winds. The authors also thank the two anonymous reviewers for their constructive and insightful comments, which in our opinion made the paper a much stronger contribution. The views, opinions, and findings contained in this report are those of the authors and should not be construed as an official National Oceanic and Atmospheric Administration or U.S. government position, policy, or decision.

APPENDIX A

Modifications to the Mueller et al. (2006) Algorithm

The inputs to the Mueller et al. (2006) algorithm (M06) include the maximum wind at flight level V_{mfl} and the radial profile of the azimuthally averaged brightness temperatures and associated standard deviations. The output includes estimates of the radius of maximum wind R_m and the wind speed at 182 km from the TC center. From V_{mfl}, R_m, and V_{182} a modified Rankine vortex:

$$V(r) = V_{\mathrm{mfl}}(R_m/r) \quad \text{for} \quad r < R_m$$

$$V(r) = V_{\mathrm{mfl}}(R_m/r)^x \quad \text{for} \quad r \geq R_m, \qquad \text{(A1)}$$

where x is the shape parameter and r is the radius from the TC center, can be used to estimate the symmetric

TABLE B1. A comprehensive list of text/binary files produced by the MTCSWA product. All files use a common naming convention, yyyyBBNN_MTCSWA_YYYYmmddHH.prd, where yyyy is the storm year, BB is the storm basin [Atlantic (AL), East Pacific (EP), Central Pacific (CP), West Pacific (WP), North Indian Ocean (IO), and Southern Hemisphere (SH)], NN is the storm number, MTCSWA is the product name, YYYY is the year of the analysis, mm is the month of the analysis, dd is the day of the analysis, HH is the hour of the analysis, and prd is the product naming convention corresponding to the contents in the rightmost column. GrADS is the Grid Analysis and Display System.

File name	File type	Contents
yyyyBBNN_MTCSWA_YYYYmmddHH.AAV	Output (ASCII)	Azimuthally averaged surface and gradient-level winds. ASCII file with header.
yyyyBBNN_MTCSWA_YYYYmmddHH.DIA	Diagnostic (ASCII)	Wind/MSLP diagnostics used for storm-surge modeling.
yyyyBBNN_MTCSWA_YYYYmmddHH.FIX	Output (ASCII)	ATCF-formatted fix that is supplied to NHC/JTWC.
yyyyBBNN_MTCSWA_YYYYmmddHH.KE	Output (ASCII)	Estimates the 0–200-km kinetic energy at flight level, the radius of maximum winds, and the surface maximum wind in the analysis.
yyyyBBNN_MTCSWA_YYYYmmddHH.LOG	Output (ASCII)	Status and latency of the various input datasets.
yyyyBBNN_MTCSWA_YYYYmmddHH.MSL	Output (ASCII)	Estimated minimum sea level pressure and the environmental sea level pressure used for the calculation.
yyyyBBNN_MTCSWA_YYYYmmddHH.SFC	Output (ASCII)	Surface wind analysis. This ASCII file contains date/time, lat, lon, and u and v (kt) on the polar analysis grid.
yyyyBBNN_MTCSWA_YYYYmmddHH.STATUS	Diagnostic (ASCII)	Information about when the analysis ran and how successful it was.
yyyyBBNN_MTCSWA_YYYYmmddHH.WIN	Output (ASCII)	Flight-level wind analysis on an azimuthal grid defined in the file.
yyyyBBNN_MTCSWA_YYYYmmddHH.bin	Output (binary, big endian)	GrADS binary file that contain gridded surface and flight-level winds.
yyyyBBNN_MTCSWA_YYYYmmddHH.ctl	Output (ASCII)	GrADS control file.
yyyyBBNN_MTCSWA_YYYYmmddHH.inp	Input (ASCII)	Contains the storm input estimates at the time of the analysis, which come from the ATCF and are generated prior to the start of the analysis.
yyyyBBNN_MTCSWA_YYYYmmddHH.obs	Input (ASCII)	Containing the winds used in the analysis. These come from IR-based flight-level analog winds, AMSU nonlinear balance winds, geostationary-based cloud and feature track winds, and scatterometry (ASCT and SCAT).
yyyyBBNN_MTCSWA_YYYYmmddHH.PEN	Input (ASCII)	Contains an estimate of environmental pressure at $r = 600$ km (usually from GFS).

wind field. The TC motion was found to cause an azimuthal wavenumber-1 asymmetry, which is linearly added to the symmetric wind field created from (A1). This is the basis for the two-dimensional flight-level wind estimates produced by M06.

It was desirable for some applications to have M06 estimate winds out to a radius of 400 km. The easiest way to do it is simply to calculate wind estimates out to 400 km using (A1), but for storms with intensities greater than 50 m s^{-1} the modified Rankine vortex creates wind estimates beyond 182 km that are too strong. To alleviate this positive bias, (A2) is introduced:

$$V(r) = V_{\mathrm{mfl}}(R_m/r)^{rx/182}. \quad \text{(A2)}$$

The symmetric winds for radii that are greater than 182 km are estimated using a linear combination of (A1) and (A2):

$$V(r) = w_{\mathrm{ol}}[V_{\mathrm{mfl}}(R_m/r)^{rx/182}] + w_{\mathrm{el}}[V_{\mathrm{mfl}}(R_m/r)^{x}], \quad \text{(A3)}$$

where

$$w_{\mathrm{ol}} = (V_{\mathrm{mfl}} - 49.4)/32.9 \quad \text{for} \quad V_{\mathrm{mfl}} \geq 50\,\mathrm{m\,s^{-1}} \quad \text{and}$$
$$w_{\mathrm{el}} = 1 - w_{\mathrm{ol}}.$$

M06 was developed using flight-level data from a sample that was biased to TCs with hurricane-force winds. This was not intentional, but rather was due to the availability of flight-level reconnaissance data. When M06 was used to estimate the wind profile of weaker TCs, those with $V_{\mathrm{mfl}} < 33$ m s^{-1}, the wind field was too peaked (i.e., x was too large) when compared with the observed winds. This is because weak TCs tend to have large R_m and broad wind fields that decrease slowly with

radius. To help to alleviate this issue, the symmetric wind field is estimated by

$$V(r) = V_{\mathrm{mfl}}(R_m/r)^{rx/182} \qquad \text{(A4)}$$

instead of (A1) when $V_{\mathrm{mfl}} < 33$ m s^{-1} and when $R_m < r < 182$ km.

APPENDIX B

Text Products

There are a number of text and binary products, in addition to the graphical products described in section 4a, that are inputs or products of the MTCSWA. These are archived on a short-term basis on the product Internet site, and operational products will be archived at NCDC. A complete list and description of these text and binary files are provided in Table B1.

REFERENCES

Bentamy, A., 2008: Characterization of ASCAT measurements based on buoy and QuikSCAT wind vector observations. *Ocean Sci. Discuss.,* **5,** 77–101.

Bessho, K., M. DeMaria, and J. A. Knaff, 2006: Tropical cyclone wind retrievals from the Advanced Microwave Sounder Unit (AMSU): Application to surface wind analysis. *J. Appl. Meteor. Climatol.,* **45,** 399–415.

Boose, E. R., K. E. Chamberland, and D. R. Foster, 2001: Landscape and regional impacts of hurricanes in New England. *Ecol. Monogr.,* Vol. 71, Ecological Society of America, 27–48.

Cobb, H. D., III, R. Knabb, P. S. Chang, and Z. Jelenak, 2008: Preliminary assessment of the utility of ASCAT ocean surface vector wind (OSVW) retrievals at the Tropical Prediction Center/National Hurricane Center. Preprints, *28th Conf. on Hurricanes and Tropical Meteorology,* Orlando, FL, Amer. Meteor. Soc., 15B.4. [Available online at http://ams.confex.com/ams/pdfpapers/137882.pdf.]

DeMaria, M., and R. W. Jones, 1993: Optimization of a hurricane track forecast model with the adjoint model equations. *Mon. Wea. Rev.,* **121,** 1730–1745.

Demuth, J., M. DeMaria, J. A. Knaff, and T. H. Vonder Haar, 2004: Validation of an Advanced Microwave Sounder Unit (AMSU) tropical cyclone intensity and size estimation algorithm. *J. Appl. Meteor.,* **43,** 282–296.

——, ——, and —— , 2006: Improvement of Advanced Microwave Sounding Unit tropical cyclone intensity and size estimation algorithms. *J. Appl. Meteor. Climatol.,* **45,** 1573–1581.

Dvorak, V. F., 1975: Tropical cyclone intensity analysis and forecasting from satellite imagery. *Mon. Wea. Rev.,* **103,** 420–430.

EUMETSAT, cited 2010: Atmospheric motion vectors factsheet, v1. EUMETSAT Doc. EUM/OPS/DOC/09/5160, 7 pp. [Available online at http://www.eumetsat.int/Home/Main/DataProducts/Atmosphere/index.htm?l=en.]

——, cited 2011: ASCAT wind product user manual, version 1.3. KNMI/EUMETSAT Doc. SAF/OSI/CDOP/KNMI/TEC/MA/126, 21 pp. [Available online at http://www.knmi.nl/publications/fulltexts/ss3_pm_ascat_1.3.pdf.]

Figa-Saldaña, J., J. J. W. Wilson, E. Attema, R. Gelsthorpe, M. R. Drinkwater, and A. Stoffelen, 2002: The Advanced Scatterometer (ASCAT) on the meteorological operational (Metop) platform: A follow on for European wind scatterometers. *Can. J. Remote Sens.,* **28,** 404–412.

Franklin, J. L., M. L. Black, and K. Valde, 2003: GPS dropwindsonde wind profiles in hurricanes and their operational implications. *Wea. Forecasting,* **18,** 32–44.

Gaiser, P. W., 2004: The WindSat space borne polarimetric microwave radiometer: Sensor description and early orbit performance. *IEEE Trans. Geosci. Remote Sens.,* **42,** 2347–2361.

Gelsthorpe, R. V., E. Schied, and J. J. W. Wilson, 2000: ASCAT—Metop's advanced scatterometer. *Eur. Space Agency Bull.,* **102,** 19–27.

Goodberlet, M. A., C. T. Swift, and J. C. Wilkerson, 1989: Remote sensing of ocean surface winds with the Special Sensor Microwave/Imager. *J. Geophys. Res.,* **94,** 14 547–14 555.

Graf, J. E., T. Wu-yang, and L. Jones, 1998: Overview of QuikSCAT mission—A quick deployment of a high resolution, wide swath scanning scatterometer for ocean wind measurement. *Proc. IEEE Southeastcon '98,* Orlando, FL, IEEE, 314–317. [Available online at http://ieeexplore.ieee.org/xpl/freeabs_all.jsp?arnumber=673359.]

Hennon, C. C., D. Long, and F. Wentz, 2006: Validation of QuikSCAT wind retrievals in tropical cyclone environments. Preprints, *14th Conf. on Satellite Meteorology and Oceanography,* Atlanta, GA, Amer. Meteor. Soc., JP1.1. [Available online at http://ams.confex.com/ams/pdfpapers/99478.pdf.]

Hollinger, J., R. Lo, G. Poe, R. Savage, and J. Pierce, 1987: The Special Sensor Microwave/Imager user's guide. 120 pp. [Available from the Naval Research Laboratory, 4555 Overlook Ave., SW, Washington, DC 20375.]

Holmlund, K., C. Velden, and M. Rohn, 2001: Enhanced automated quality control applied to high-density satellite-derived winds. *Mon. Wea. Rev.,* **129,** 517–529.

Knaff, J. A., and R. M. Zehr, 2007: Reexamination of tropical cyclone wind–pressure relationships. *Wea. Forecasting,* **22,** 71–88.

——, and B. A. Harper, 2010: Tropical cyclone surface wind structure and wind-pressure relationships. *Proc. WMO Int. Workshop on Tropical Cyclones—VII,* La Reunion, France, WMO, KN1, 35 pp. [Available online at http://www.wmo.int/pages/prog/arep/wwrp/tmr/otherfileformats/documents/KN1.pdf.]

——, R. M. Zehr, M. D. Goldberg, and S. Q. Kidder, 2000: An example of temperature structure differences in two cyclone systems derived from the Advance Microwave Sounder Unit. *Wea. Forecasting,* **15,** 476–483.

——, C. R. Sampson, M. DeMaria, T. P. Marchok, J. M. Gross, and C. J. McAdie, 2007: Statistical tropical cyclone wind radii prediction using climatology and persistence. *Wea. Forecasting,* **22,** 781–791.

Kossin, J. P., J. A. Knaff, H. I. Berger, D. C. Herndon, T. A. Cram, C. S. Velden, R. J. Murnane, and J. D. Hawkins, 2007: Estimating hurricane wind structure in the absence of aircraft reconnaissance. *Wea. Forecasting,* **22,** 89–101.

Maclay, K. S., M. DeMaria, and T. H. Vonder Haar, 2008: Tropical cyclone inner core kinetic energy evolution. *Mon. Wea. Rev.,* **136,** 4882–4898.

Mueller, K. J., M. DeMaria, J. A. Knaff, J. P. Kossin, and T. H. Vonder Haar, 2006: Objective estimation of tropical cyclone wind structure from infrared satellite data. *Wea. Forecasting,* **21,** 990–1005.

NHC, cited 2011: National Hurricane Center Forecast Verification (Text), Section 2. [Available online at http://www.nhc.noaa.gov/verification/verify2.shtml?text.]

Pielke, R. A., Jr., J. Gratz, C. W. Landsea, D. Collins, M. Saunders, and R. Musulin, 2008: Normalized hurricane damages in the United States: 1900–2005. *Nat. Hazards Rev.,* **9,** 29–42.

Powell, M. D., and T. A. Reinhold, 2007: Tropical cyclone destructive potential by integrated kinetic energy. *Bull. Amer. Meteor. Soc.,* **88,** 513–526.

——, S. H. Houston, L. R. Amat, and N. Morisseau-Leroy, 1998: The HRD real-time hurricane wind analysis system. *J. Wind Eng. Ind. Aerodyn.,* 77-78, 53–64.

——, and Coauthors, 2010: Reconstruction of Hurricane Katrina's wind fields for storm surge and wave hindcasting. *Ocean Eng.,* **37,** 26–36.

Rappaport, E. N., and Coauthors, 2009: Advances and challenges at the National Hurricane Center. *Wea. Forecasting,* **24,** 395–419.

Sampson, C. R., and A. J. Schrader, 2000: The Automated Tropical Cyclone Forecasting System (version 3.2). *Bull. Amer. Meteor. Soc.,* **81,** 1231–1240.

Thacker, W. C., 1988: Fitting models to inadequate data by enforcing spatial and temporal smoothing. *J. Geophys. Res.,* **93,** 10 655–10 665.

Velden, C. S., C. M. Hayden, S. J. Nieman, W. P. Menzel, S. Wanzong, and J. S. Goerss, 1997: Upper-tropospheric winds derived from geostationary satellite water vapor observations. *Bull. Amer. Meteor. Soc.,* **78,** 173–195.

——, T. L. Olander, and S. Wanzong, 1998: The impact of multispectral *GOES-8* wind information on Atlantic tropical cyclone track forecasts in 1995. Part I: Dataset methodology, description, and case analysis. *Mon. Wea. Rev.,* **126,** 1202–1218.

——, and Coauthors, 2005: Recent innovations in deriving tropospheric winds from meteorological satellites. *Bull. Amer. Meteor. Soc.,* **86,** 205–223.

Zehr, R. M., and J. A. Knaff, 2007: Atlantic major hurricanes, 1995–2005—Characteristics based on best-track, aircraft, and IR images. *J. Climate,* **20,** 5865–5888.